Type of contribution:
Editorial
▶ Research Paper
Case Study
Review Paper
Scientific Data
Report of Tech. Application

mesi
e-issn. 2798-5245
Mechanical Engineering
for Society and Industry
Vol. 5, No. 1 (2025) pp 158-168
https://doi.org/10.31603/mesi.12581

Advanced computational techniques for predicting 3D printing distortion in selective laser melting processes of Aluminium AlSi10Mg

Moch. Agus Choiron[1]*, Anindito Purnowidodo[1], Achfas Zacoeb[2], Gembong Edhi Setyawan[3], Willy Artha Wirawan[4], Yudhi Ariadi[5], Allan E.W. Rennie[6], Diva Kurnianingtyas[3]

[1] Department of Mechanical Engineering, Universitas Brawijaya, Malang 65145, **Indonesia**
[2] Department of Civil Engineering, Universitas Brawijaya, Malang 65145, **Indonesia**
[3] Department of Computer Science, Universitas Brawijaya, Malang 65145, **Indonesia**
[4] Department of Aircraft Maintenance Engineering, Politeknik Penerbangan Surabaya, Surabaya 60236, **Indonesia**
[5] School of Engineering, University of Warwick, Library Rd, Coventry CV4 7AL, **United Kingdom**
[6] School of Engineering, Lancaster University, Lancaster LA1 4YW, **United Kingdom**
✉ agus_choiron@ub.ac.id

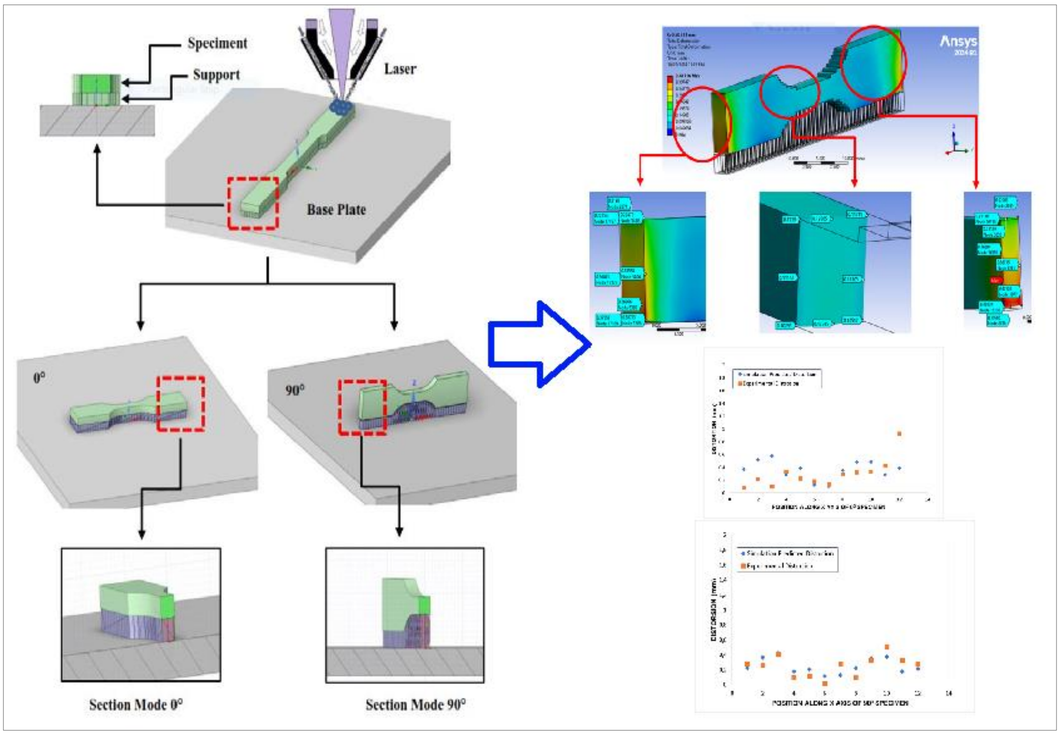

Highlights:

- FEM accurately predicts distortion in SLM-process AlSi10Mg parts.
- Scanning orientation critically affects distortion with 90° orientation reducing distortion.
- Optimal scan orientation improves mechanical properties, balancing strength and flexibility.
- This study optimizes SLM parameters for precise and stable metal parts in high-demand industries.

Article info
Submitted:
2024-10-30
Revised:
2025-05-27
Accepted:
2025-06-04

Publisher
Universitas Muhammadiyah Magelang

Abstract

Distortion for 3D printing using Selective Laser Melting (SLM) on AlSi10Mg aluminium is an important issue that affects the final manufactured product. This research aims to develop a finite element method (FEM)-based computational simulation and experimental validation to predict distortion in 3D printed products using SLM. The study results found that the variation of 3D printing position affects the resulting product's distortion and mechanical properties. The 90° part print position results in smaller distortion of 0.303 and 0.335 mm than the 0° part print position of 0.329 and 0.378, respectively, making it more suitable for high-precision applications. This study confirms the importance of scan orientation in controlling distortion in the SLM process, which can be used as a guide for optimal printing parameters. With proper orientation selection, the risk of distortion or defects in SLM products can be minimised, and industrial production efficiency can be improved.

Keywords: SLM; Laser powder; 3D printing; Distortion; Additive manufacturing; Finite element method

1. Introduction

In recent years, 3D printing technology, particularly the SLM method, has emerged as an innovative solution within the manufacturing industry, enabling the fabrication of metal components with intricate geometric complexity [1], [2]. The application of the aluminium alloy AlSi10Mg, processed via a layer-by-layer high-energy laser melting technique, yields components that are both lightweight and mechanically robust. Consequently, SLM has gained considerable traction across diverse sectors, including automotive, aerospace, and general manufacturing [3]. Nonetheless, the SLM process frequently encounters significant challenges, such as distortion during printing, which can adversely impact the dimensional accuracy and mechanical properties of the final products [4], [5].

Thermal distortion is one of the primary obstacles, introducing uncertainties in the printing outcomes and increasing the risk of defects [6], [7]. This distortion is primarily driven by rapid temperature fluctuations and thermal instability, potentially leading to product failure and increased production costs [8]. Recent studies have contributed to developing predictive models to understand the distortion characteristics in metals such as nickel and titanium during the SLM process [3], [9], [10]. However, these studies often do not explicitly explore the interaction between dynamic processing parameters, such as laser scanning speed and input energy, with the material's thermo-mechanical behaviour. Furthermore, many approaches still rely heavily on direct experimentation, which is time-consuming and costly. As a result, computational simulations remain an appealing alternative for predicting thermal and mechanical behaviour during the SLM process.

Several studies have sought to develop thermal simulation models for predicting distortion in metals processed by Selective Laser Melting (SLM); however, significant limitations persist. Many models emphasize temperature distribution but neglect the critical interaction between thermal and mechanical effects, such as residual stress formation during cooling, which significantly influences print distortion [11]. Moreover, existing computational models frequently overlook the anisotropic behavior of materials, especially alloys like AlSi10Mg, which experience substantial microstructural and mechanical property changes throughout the multi-layer printing process [4], [10], [12].

AlSi10Mg is widely used in both SLM research and industrial applications due to its advantageous combination of lightweight characteristics, high strength, excellent corrosion resistance, and good thermal conductivity [13], [14]. These properties make it particularly suitable for aerospace, automotive, and biomedical components. Additionally, its relatively favorable printability and mechanical performance after SLM processing establish AlSi10Mg as a benchmark material for investigating distortion and residual stresses in metal additive manufacturing [15], [16], [17].

Current modeling approaches also inadequately represent more complex thermomechanical phenomena essential for precise predictions in specific alloys such as steel [18], [19], [20]. Although efforts have been made to simulate distortion across various metal materials, comprehensive models that specifically address the unique features of materials like AlSi10Mg within the SLM context remain underdeveloped. Furthermore, optimization of process parameters such as laser speed and scanning path to minimize distortion often relies solely on thermal analysis, disregarding broader mechanical interactions [8], [21]. To overcome these shortcomings, a model integrating thermal, mechanical, and anisotropic factors is necessary to improve distortion prediction accuracy during the SLM process.

Therefore, advanced computational techniques are essential for predicting distortion in SLM. This study aims to comprehensively evaluate simulation models capable of effectively integrating simultaneous thermal and mechanical effects on AlSi10Mg material. The findings, including temperature distortion, heat distribution, stress, and strain, are expected to improve the final product quality in SLM and contribute significantly to high-precision manufacturing applications.

2. Material and Method

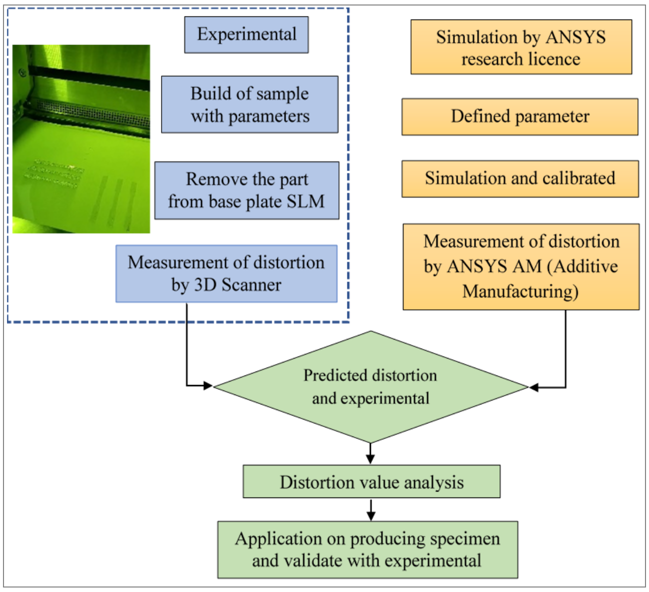

Figure 1. Simulation and experiment approach of the current study

A finite element method based simulation tool using ANSYS Additive Manufacturing 2024 R1 Research license has been selected to model and analyse tensile test specimen products using AlSi10Mg aluminium material. Simulation using a modelling approach is used to predict the distortion in SLM products. The plot of simulation results was observed as a criterion for determining the amount of distortion that occurred. The optimum model was validated experimentally using the 3D Scanner machine. For more details, the procedure of this research approach is presented in **Figure 1**.

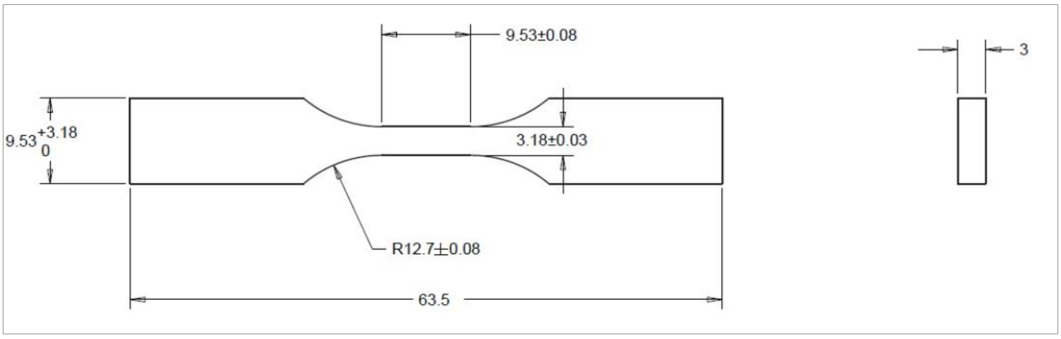

Figure 2. Geometry model of tensile test specimen

2.1. Computational Simulation based on FEM

In this study, specimens were made with two variations of part positions, 0° and 90°. The CAD model of the AlSi10Mg Aluminium Tensile test specimen was created with dimensions as shown in **Figure 2**. The mechanical properties of AlSi10Mg aluminium alloy were determined as presented in **Table 1**. A body-fitted Cartesian measuring type of 0.5 mm was used in the constructed components to minimise the simulation process. For the base plate, hexadominant meshing of 4 mm size with 21320 elements and 3mm distance to the part was used. More details of the simulation modelling scheme carried out in the study can be seen in **Figure 3**.

The material Aluminium AlSi10Mg was selected for this study due to its superior mechanical and thermal properties, as well as its suitability for high-precision engineering applications such as Selective Laser Melting (SLM). To provide a comprehensive understanding of the characteristics of this material, the complete specifications of Aluminium AlSi10Mg are presented in **Table 1**.

Table 1. Specification Alumunium AlSi10Mg

Density (kg/m³)	Modulus Elasticity (MPa)	Poisson's ratio	Yields Strength (MPa)	Tangent Modulus (Mpa)	Specific Heat
2700	65000	0.33	60.7	450	896

2.2. Experimental Study

This study's tensile test specimen geometry was made using an Eplus3D EP-M260 Metal 3D Printer machine. The AlSi10Mg aluminium alloy was atomised with argon gas. The laser firing distance on the base plate was set at 150 mm, and samples were made sequentially with part positions of 0° and 90°. To maintain data validity, the 3D printing process of each specimen was

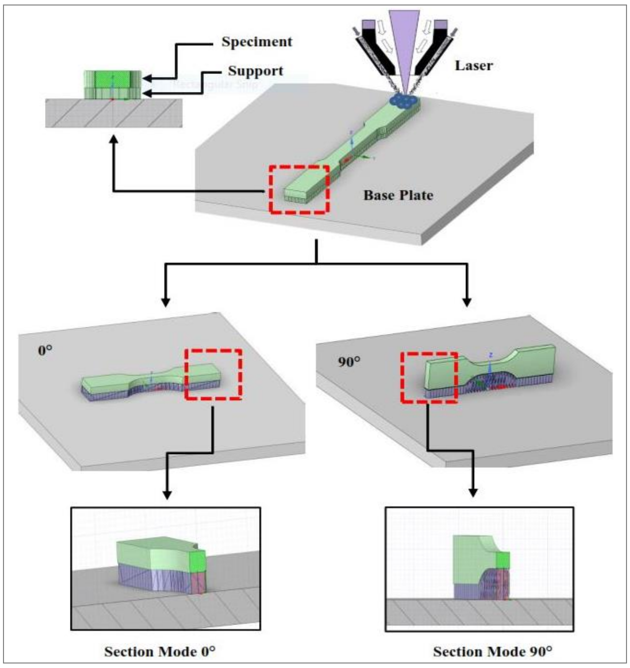

Figure 3. Additive manufacturing modelling

repeated three times. Furthermore, the 3D printing results were evaluated using a FARO Quantum M MAX 2.5m 7 axis 3D scanner. Distortion was measured at several specimen points from the overall length of the printed tensile test specimen.

2.3. Tensile Strength Test

The results of tensile test specimens that have been printed using Eplus3D EP-M260 Metal 3D Printer machine at variations of 0° and 90° scanning patterns are then tested using a Universal Tensile Material machine model VTS-WDW 300E with a speed of 1 mm/minutes. The specimen fractures were observed using a Canon EOS 1300D 18-55mm IS F3.5-5.6ISII digital camera.

3. Results and Discussion

3.1. Simulation and Experiment Distortion

From the simulation using ANSYS in the Additive Manufacturing process with variations in part position, the maximum distortion value was obtained with a part position of 90° to the base of 0.303 mm and 0.329 mm at position 0°. The different position of the parts in the SLM process causes variations in heat distribution, cooling, stress distribution, and gravitational influence, all of which contribute to the distortion presented in **Figure 4** and **Figure 5**. The lower distortion at 0° position compared to 90° can be attributed to the more even heat distribution, faster cooling process, and more well-distributed gravitational force.

Simulation analysis indicates that at a 90° orientation, the component's contact surface with the base is smaller compared to the 0° orientation (**Figure 6** to **Figure 8**). During the removal support step, the maximum distortion observed at 90° was 0.447 mm, while at 0°, it reached 0.606 mm. This support configuration leads to a more localized heat distribution and slower cooling, as heat dissipates through a smaller contact area with the base. Conversely, at 90°, the larger contact area with the base promotes more efficient heat distribution and faster cooling, which contributes to a reduction in distortion. Additionally, it is noted that gravity acting on parts oriented more perpendicular to the newly deposited layer can induce slight bending or deflection, thereby increasing distortion. In contrast, at 90°, the gravitational force aligns parallel to the base, allowing the component to better retain its shape without significant bending or distortion [12]. In addition, the expansion and contraction of the material due to heating and cooling are more likely to occur in the horizontal direction, causing more significant deformation of the part. The residual stress distribution is evener in the vertical position due to the larger contact area with the base. This helps

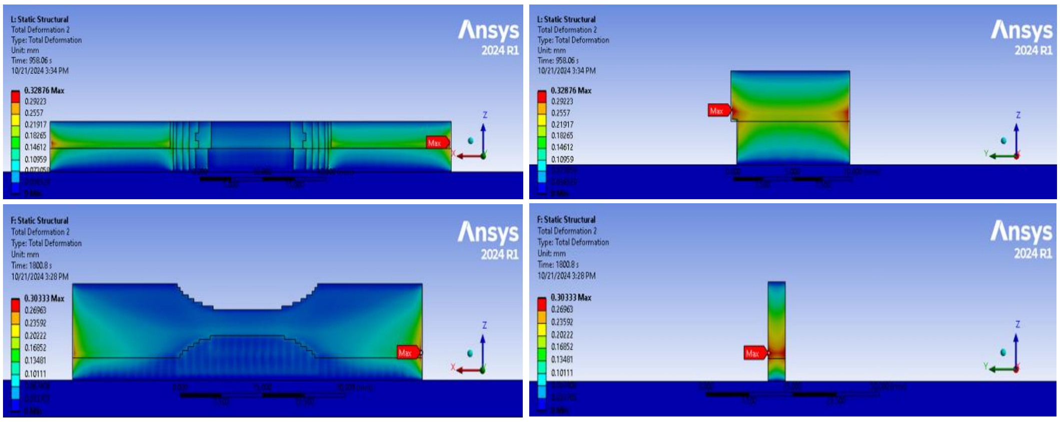

Figure 4. The simulation predicted distortion part (build step)

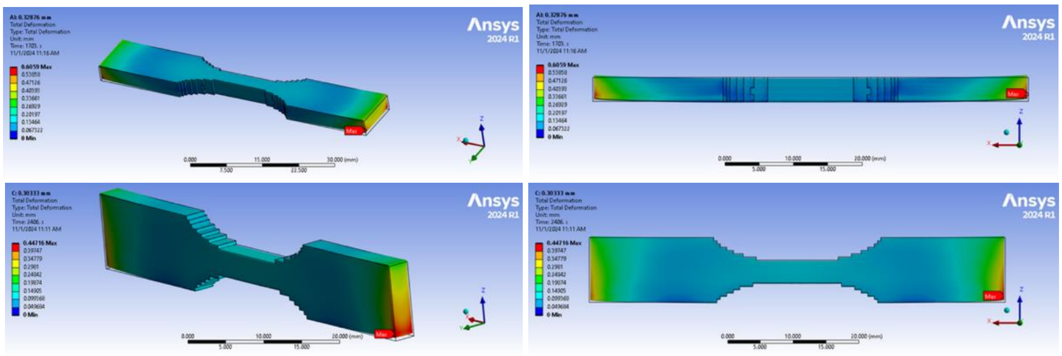

Figure 5. The simulation predicted distortion part (removal support step)

balance the stresses and reduces the possibility of distortion. Contraction and expansion occur more evenly because the part is better aligned with the base, so its shape tends to be more stable during cooling [10], [22].

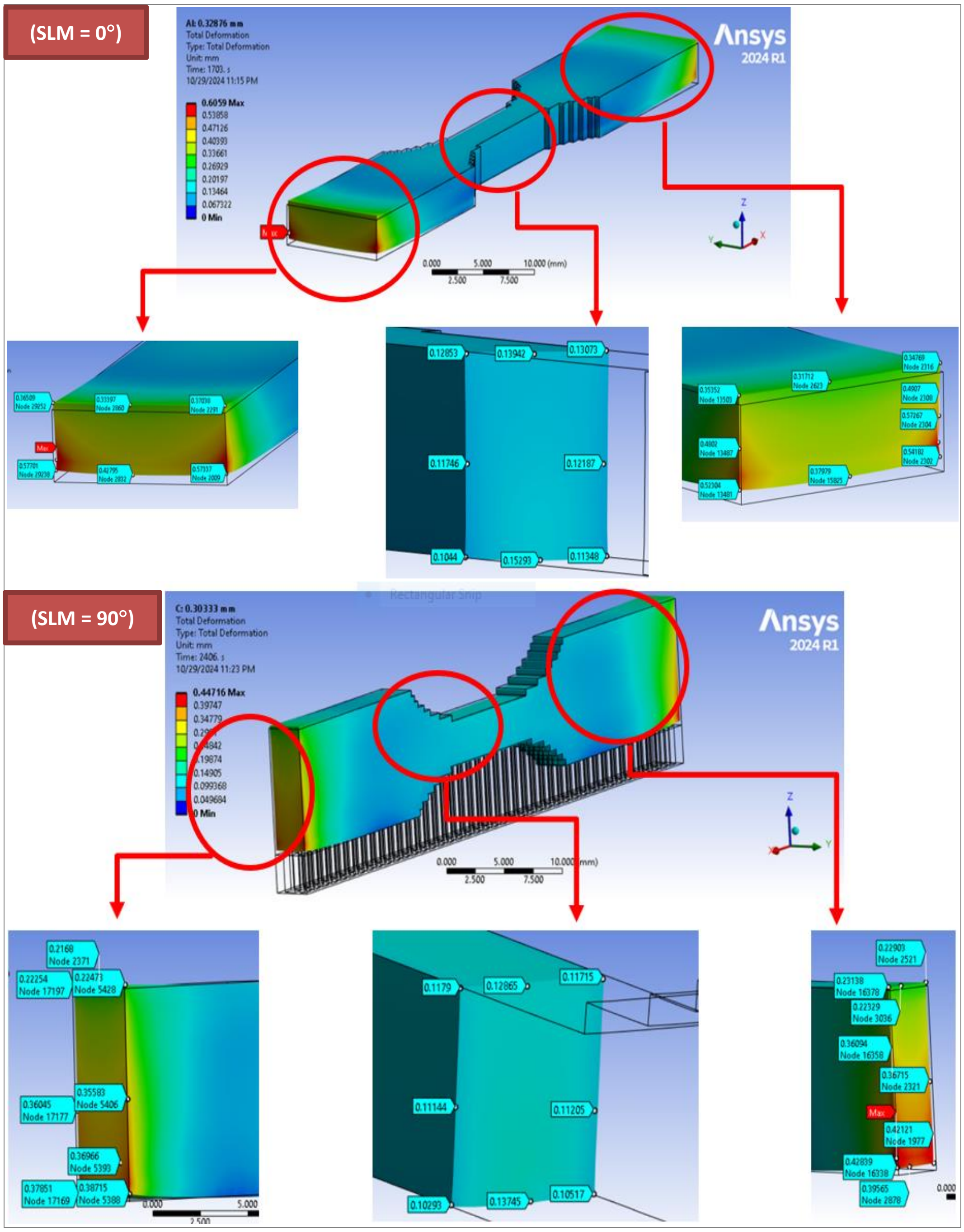

Figure 6. The simulation predicted distortion Support 0° and 90°

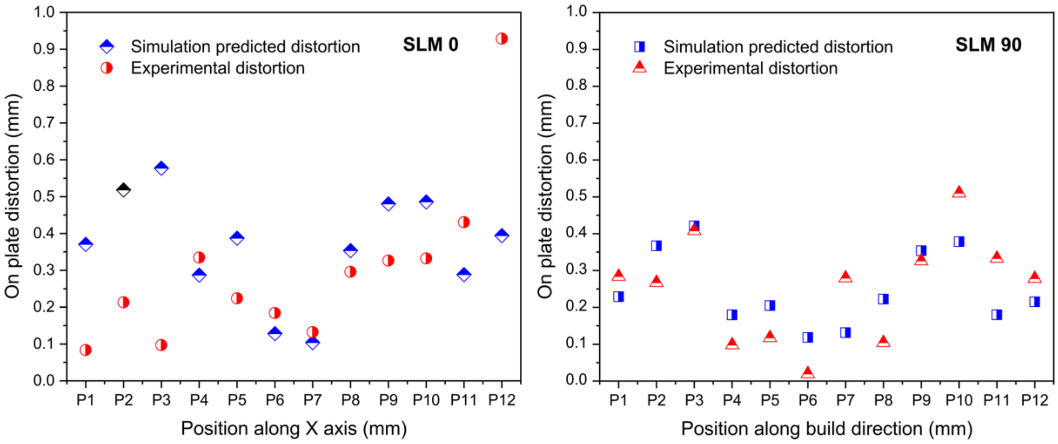

Figure 7. Simulation and experiment removal support step

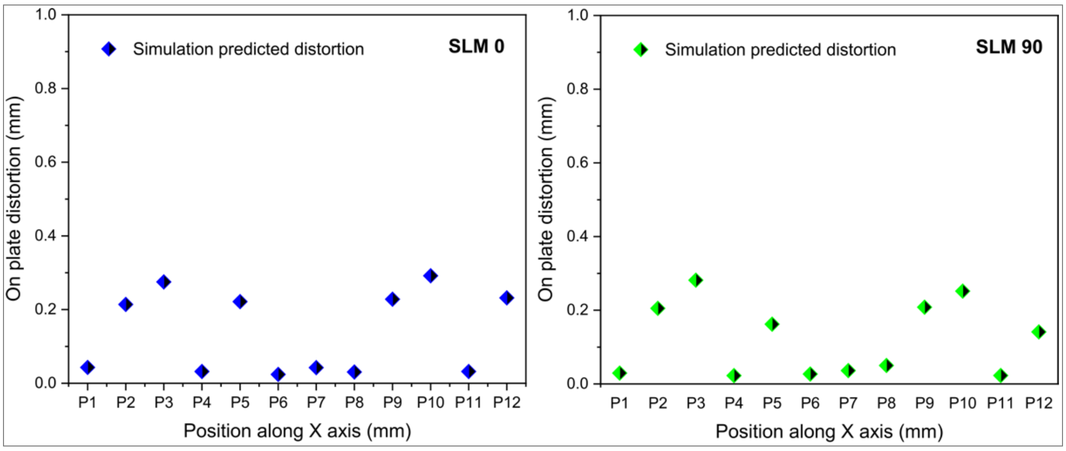

Figure 8. Simulation distortion built step

The distortion analysis of specimens scanned at a 90° orientation reveals a more uniform distribution of distortion along the specimen length. The experimental and simulation results indicate relatively consistent distortion values across multiple measurement points, with only minor differences observed. This uniform distortion pattern is attributed to the cross-hatch scanning strategy employed at the 90° orientation, which promotes more even heat distribution during the manufacturing process. As a result, localized thermal stresses are minimized, thereby reducing significant deformation in specific regions.

Quantitatively, the mean distortion values along the X-axis for the 90° orientation are 0.2521 mm (experimental) and 0.2502 mm (simulation) (**Table 2**). The low standard deviations 0.0446 mm for experimental data and 0.0635 mm for simulation—further confirm minimal variation in distortion across measurement points. The strong agreement between simulation and experimental results validates the accuracy of the simulation model in capturing the underlying thermal and mechanical behaviors associated with the 90° scanning configuration. This confirms the model's reliability in predicting distortion distribution and supports its application for process optimization. In contrast, specimens scanned at 0° exhibit markedly different distortion characteristics, with higher average distortion values of 0.2985 mm (experimental) and 0.3645 mm

Table 2. Comparison of simulated and experimental distortion

Position along X axis (mm)	0°			90°		
	Simulation	Experiment	Stdev	Simulation	Experiment	Stdev
P1	0.37038	0.0834	0.2029255	0.22903	0.284	0.03887
P2	0.51834	0.213	0.21590798	0.36715	0.2671	0.070746
P3	0.57701	0.0971	0.33934762	0.42121	0.4078	0.009482
P4	0.28701	0.3347	0.03372192	0.17985	0.098	0.057877
P5	0.38724	0.2239	0.11549882	0.20491	0.1174	0.061879
P6	0.12821	0.1839	0.03937878	0.11837	0.0195	0.069912
P7	0.10381	0.1322	0.02007476	0.13146	0.2795	0.10468
P8	0.35352	0.2958	0.0408142	0.22254	0.1043	0.083608
P9	0.4802	0.3264	0.10875302	0.35373	0.3262	0.019467
P10	0.48566	0.3323	0.1084419	0.37851	0.5101	0.093048
P11	0.28834	0.4306	0.10059301	0.18012	0.333	0.108102
P12	0.39425	0.9287	0.37791322	0.21517	0.2782	0.044569
Average	0.3644975	0.2985	0.14194756	0.250170833	0.252091667	0.06352

(simulation). The simulation standard deviation of 0.1419 mm notably exceeds the experimental standard deviation of 0.1155 mm, indicating greater variability in distortion across measurement points. The maximum experimental distortion observed at point P12 reaches 0.9287 mm, highlighting pronounced inhomogeneity in distortion for this orientation.

The increased and uneven distortion observed in the 0° orientation results from the unidirectional scanning pattern, which produces an imbalanced thermal field and uneven heat distribution. This induces localized thermal stress accumulation and elevates the risk of excessive deformation in certain regions. Moreover, the simulation tends to underestimate distortion at specific points relative to experimental measurements, revealing limitations of the model in fully representing the complex thermal-mechanical interactions occurring during processing. The unidirectional heat flow generates steep temperature gradients that exacerbate distortion and compromise the dimensional accuracy of the final product [23], [24].

The comparison between the two scanning orientations emphasizes the critical influence of scanning strategy on distortion behavior. The 90° cross-hatch orientation provides lower and more uniform distortion due to balanced thermal input, making it preferable for applications requiring high dimensional stability and precise deformation control. Conversely, the 0° orientation, characterized by a unidirectional pattern, leads to higher and more heterogeneous distortion, rendering it less suitable for components with stringent tolerance requirements. Therefore, the 90° scan orientation is recommended for manufacturing processes that demand strict control over deformation and dimensional accuracy. When the 0° orientation is necessary, advanced process control strategies such as optimization of scanning parameters or enhanced cooling techniques should be implemented to mitigate distortion. Additionally, improving the fidelity of simulation models is essential for accurately predicting distortion under conditions that generate uneven patterns, such as the 0° scan orientation.

3.2. Tensile Strength

Analyses of the tensile test results of AlSi10Mg specimens moulded using the Selective Laser Melting (SLM) method with laser scanning angles of 0° and 90° revealed stress-strain curves showing significant differences in the strength and elasticity of the material due to variations in scanning orientation, as presented in **Figure 9**.

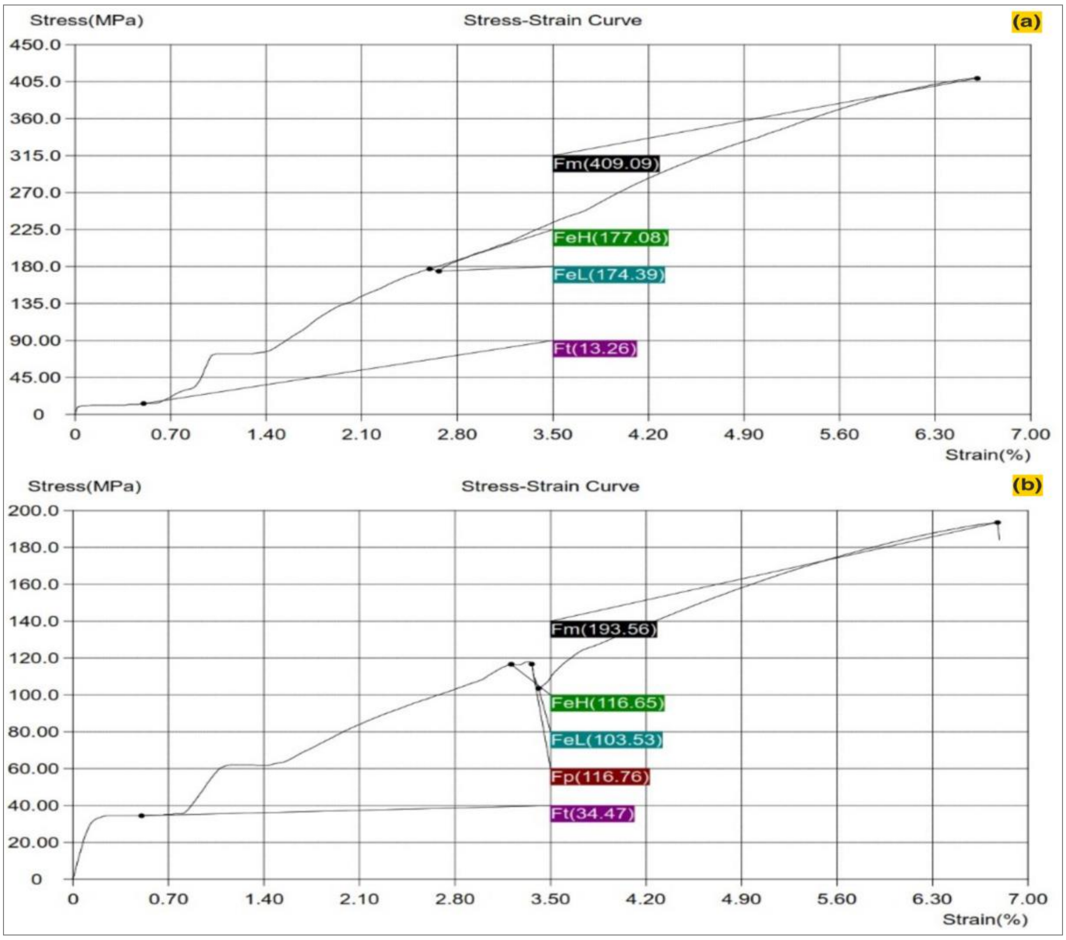

Figure 9. Stress-strain: (a) SLM 0-0° (b) SLM 0-90°

The specimen with a Scanning Orientation of 0° showed a high maximum stress (Fm) of 409.09 MPa, indicating that the material has excellent tensile strength at this orientation. The upper (FeH) and lower (FeL) elastic stresses were recorded at 177.08 MPa and 174.39 MPa, respectively, indicating that this material has a high elastic limit before entering plastic deformation. The initial tensile stress value (Ft) was 13.26 MPa, indicating moderate initial resistance to early deformation. This specimen achieved an elongation strain of approximately 6.30%, indicating the ability to undergo moderate plastic deformation before fracture. From these characteristics, it can be concluded that the 0° scan orientation can provide optimal tensile strength with the risk of brittle fracture that may occur under extreme loading conditions. This orientation is ideal for structural applications that require high tensile strength with limited deformation [25], [26].

In comparison, the Specimen with a 90° Scanning Orientation showed a lower maximum stress of 193.56 MPa. This value indicates that the material's tensile strength at 90° orientation is lower than that at 0° orientation. The upper (FeH) and lower (FeL) elastic stresses recorded in this specimen are 116.65 MPa and 103.53 MPa, respectively, lower than the 0° specimen, indicating a lower elastic limit of the material. However, the initial tensile stress (Ft) value of 34.47 MPa indicates a higher initial resistance to initial deformation than the 0° specimen. In addition, this specimen elongated to about 7.00%, which means better plastic deformation capability. From these results, the 90° scan orientation seems more suitable for applications requiring more excellent plastic deformation capability without requiring extremely high tensile strength [25].

A comparison of the results of these two specimens shows that the laser scanning orientation in the SLM process significantly influences the mechanical properties of the resulting material. The 0° scanning orientation provides higher tensile strength and greater elastic limit, which is suitable for applications that require structural strength and resistance to high tensile loads. On the other hand, a scan orientation of 90° produces materials with higher elasticity, which is more suitable for applications that require more significant plastic deformation and flexibility in resisting strain without the risk of sudden fracture. These results demonstrate the importance of scan orientation selection in metal moulding processes using SLM to optimise the mechanical properties of materials according to application requirements [26].

3.3. Macro Photo of Specimens Fracture

Figure 10 shows a fracture in a specimen with a scanning angle of 0°, which is shown to have a rough fracture surface with uncertain contours. This fracture surface indicates a brittle fracture

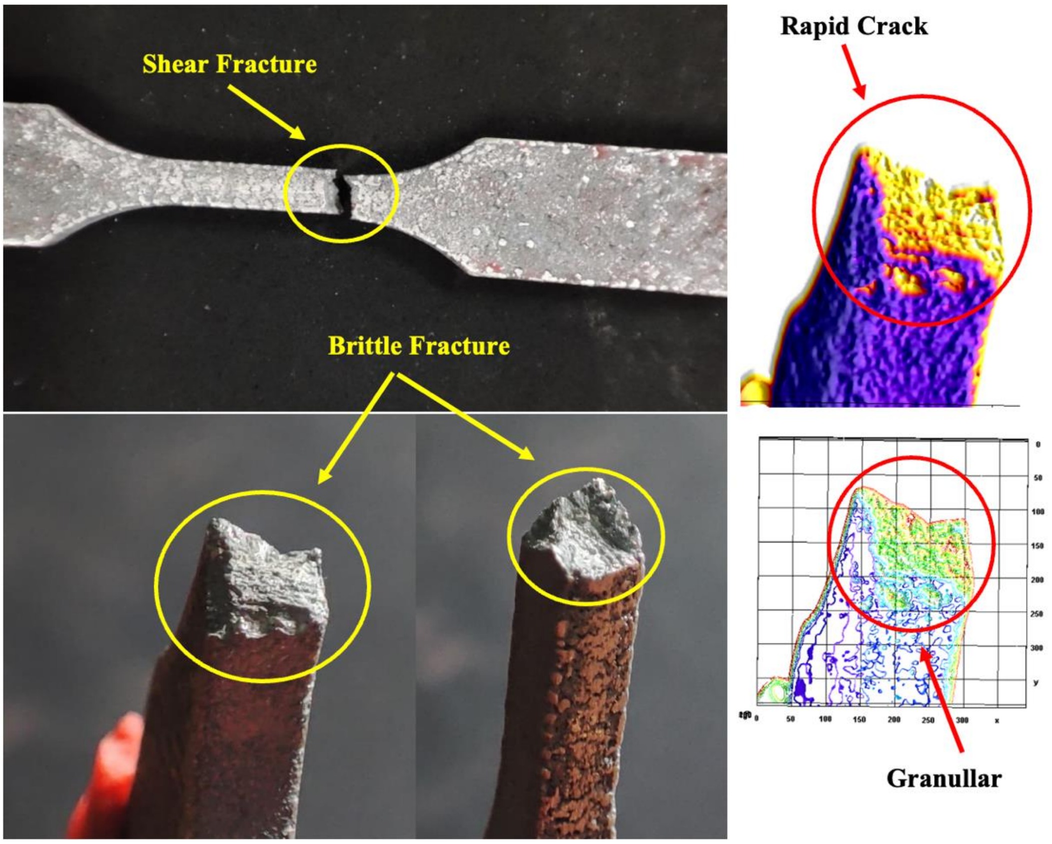

Figure 10. Specimen fracture SLM SLM 0°

with pointed and bright characteristics. This structure suggests that the applied tensile force caused a fracture in the specimen. The 0° orientation indicates that the moulded layers are arranged parallel without significant angle variation, potentially reducing the bond between layers. As a result, the tensile strength of these specimens may be decreased as the bonds between the layers are not as strong as those formed at orientations with more diverse angles. As such, these specimens are prone to brittle fracture as the tensile force is directly directed along the direction of the weak bond [27].

The fracture in the specimen with a 90° scan angle shows a more varied surface and indications of more Complex Disruption (**Figure 11**). This different fault surface from the 0° specimen may indicate that the 90° orientation provides better cohesion between layers, with some parts of the fault showing a stronger bond between layers. In the 90° orientation, the different angles between the layers allow the tensile forces to be distributed more evenly and increase the resistance to early cracking. This leads to slower deformation; some areas may experience plastic deformation before the fracture is fully established. Overall, specimens with a 0-90° orientation tend to have more tensile fracture characteristics, which suggests that this orientation is more suitable for applications that require better resistance to tensile forces.

Specimens with a 90° orientation show better tensile strength potential and stronger resistance to fracture compared to specimens with a 0° orientation. This orientation distributes the tensile stress better and improves cohesion between layers. In the context of 3D metal printing for structural applications, choosing the proper scan angle can improve the mechanical performance of the mould, mainly when used in applications subjected to constant or cyclical tensile loading [28].

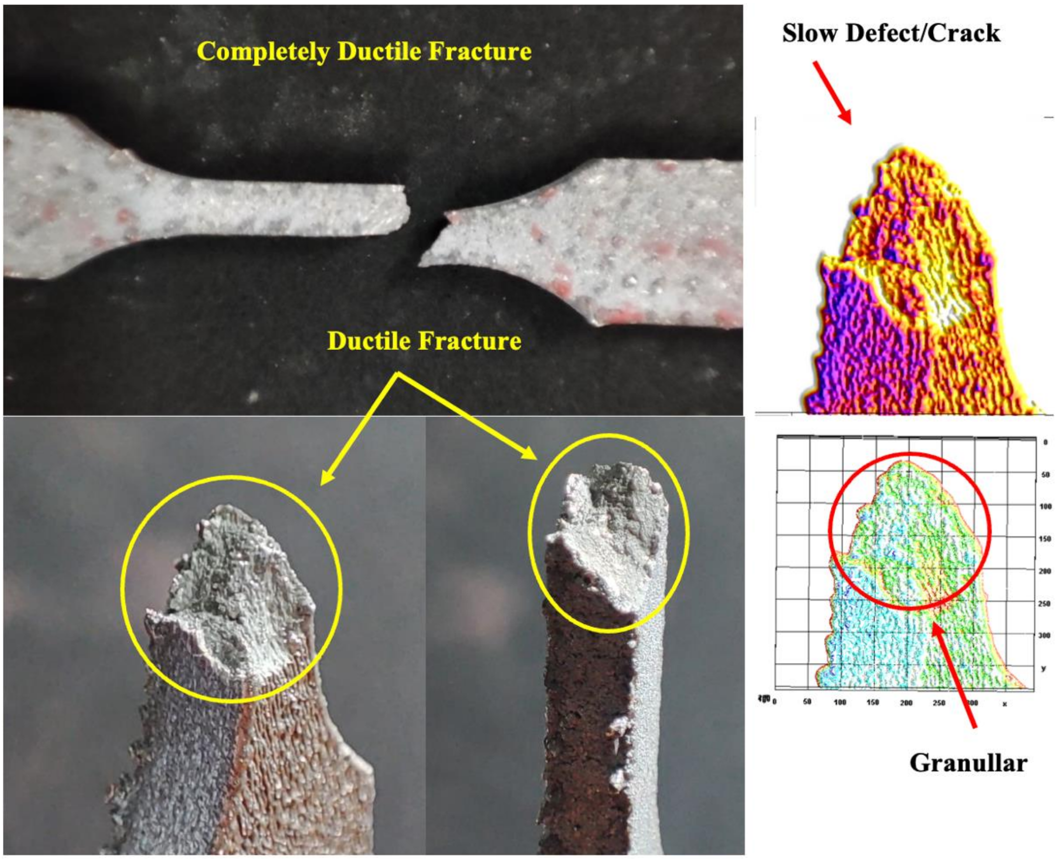

Figure 11. Specimen fracture SLM SLM 90°

4. Conclusion

Comparison between simulation and experimental results shows that the laser scanning orientation significantly influences the distortion pattern in AlSi10Mg SLM-printed specimens. The 90° scanning orientation results in more even distortion and lower values of 0.303; 0.335 mm compared to the 0° orientation of 0.329; 0.378 mm, making it a more suggestion choice for applications with a high degree of dimensional control. These results are essential to promote the adoption of moulding parameter settings in the SLM process to improve print quality and product dimensional stability, which are critical in industrial applications that require high tolerance to distortion.

Authors' Declaration

Authors' contributions and responsibilities - M.A.C., A.P.: The authors made substantial contributions to the conception and design of the study; A.Z., G.E.S., W.A.W., DK: The authors took responsibility for data analysis, interpretation, and discussion of results; Y.A., A.E.W.R.: The authors read and approved the final manuscript.

Funding –*DOKAR (Dosen Berkarya)* Programme and Research Development FTUB 2024.

Availability of data and materials - All data is available from the authors.

Competing interests - The authors declare no competing interests.

Additional information – No additional information from the authors.

References

[1] J. S, R. M, S. P. AVS, N. B K, and C. U, "Study of residual stresses and distortions from the Ti6Al4V based thin-walled geometries built using LPBF process," *Defence Technology*, vol. 28, pp. 33–41, 2023, doi: 10.1016/j.dt.2023.01.002.

[2] A. Y. Alqutaibi, M. A. Alghauli, M. H. A. Aljohani, and M. S. Zafar, "Advanced additive manufacturing in implant dentistry: 3D printing technologies, printable materials, current applications and future requirements," *Bioprinting*, vol. 42, no. August, p. e00356, 2024, doi: 10.1016/j.bprint.2024.e00356.

[3] S. Ghosh, J. Zollinger, M. Zaloznik, D. Banerjee, C. K. Newman, and R. Arroyave, "Modeling of hierarchical solidification microstructures in metal additive manufacturing: Challenges and opportunities," *Additive Manufacturing*, vol. 78, no. June, p. 103845, 2023, doi: 10.1016/j.addma.2023.103845.

[4] Y. Li, K. Zhou, P. Tan, S. B. Tor, C. K. Chua, and K. F. Leong, "Modeling temperature and residual stress fields in selective laser melting," *International Journal of Mechanical Sciences*, vol. 136, no. December 2017, pp. 24–35, 2018, doi: 10.1016/j.ijmecsci.2017.12.001.

[5] R. Konečná, G. Nicoletto, L. Kunz, and A. Bača, "Microstructure and directional fatigue behavior of Inconel 718 produced by selective laser melting," *Procedia Structural Integrity*, vol. 2, pp. 2381–2388, 2016, doi: 10.1016/j.prostr.2016.06.298.

[6] K. Ökten and A. Biyikoğlu, "Development of thermal model for the determination of SLM process parameters," *Optics & Laser Technology*, vol. 137, p. 106825, May 2021, doi: 10.1016/j.optlastec.2020.106825.

[7] K. Prem Ananth and N. D. Jayram, "A comprehensive review of 3D printing techniques for biomaterial-based scaffold fabrication in bone tissue engineering," *Annals of 3D Printed Medicine*, vol. 13, p. 100141, 2024, doi: 10.1016/j.stlm.2023.100141.

[8] A. Shrivastava, S. Anand Kumar, and S. Rao, "A numerical modelling approach for prediction of distortion in LPBF processed Inconel 718," *Materials Today: Proceedings*, vol. 44, pp. 4233–4238, 2020, doi: 10.1016/j.matpr.2020.10.538.

[9] C. Yu *et al.*, "Selective laser melting of GH3536 superalloy: Microstructure, mechanical properties, and hydrocyclone manufacturing," *Advanced Powder Materials*, vol. 3, no. 1, p. 100134, 2024, doi: 10.1016/j.apmate.2023.100134.

[10] D. Xie *et al.*, "A Review on Distortion and Residual Stress in Additive Manufacturing," *Chinese Journal of Mechanical Engineering: Additive Manufacturing Frontiers*, vol. 1, no. 3, p. 100039, 2022, doi: 10.1016/j.cjmeam.2022.100039.

[11] Y. Huang, L. J. Yang, X. Z. Du, and Y. P. Yang, "Finite element analysis of thermal behavior of metal powder during selective laser melting," *International Journal of Thermal Sciences*, vol. 104, pp. 146–157, 2016, doi: 10.1016/j.ijthermalsci.2016.01.007.

[12] D. Sarkar, A. Kapil, and A. Sharma, "Advances in computational modeling for laser powder bed fusion additive manufacturing: A comprehensive review of finite element techniques and strategies," *Additive Manufacturing*, vol. 85, no. October 2023, p. 104157, 2024, doi:

10.1016/j.addma.2024.104157.

[13] L. Zhuo *et al.*, “Microstructural evolution and performance optimization of SLM-fabricated W/AlSi10Mg composites,” *Journal of Alloys and Compounds*, vol. 1010, no. October 2024, p. 178317, 2025, doi: 10.1016/j.jallcom.2024.178317.

[14] C. Li *et al.*, “Effect of strontium salt modification on the microstructure and creep properties of SLM-formed SiC/AlSi10Mg composites,” *Journal of Materials Research and Technology*, vol. 35, no. December 2024, pp. 5455–5463, 2025, doi: 10.1016/j.jmrt.2025.02.194.

[15] C. Zhang, B. Chen, H. M. Li, X. Liu, G. Zhou, and G. Gou, “Propagation characteristics of ultrasonic in SLM manufactured AlSi10Mg,” *Ultrasonics*, vol. 135, no. June, p. 107134, 2023, doi: 10.1016/j.ultras.2023.107134.

[16] K. Chen, Q. Lu, X. Yong, P. Zhang, H. Yan, and H. Shi, “Process parameter optimization of SLM AlSi10Mg based on Box-Behnken design and experimental study on microstructure and mechanical properties,” *Materials Today Communications*, vol. 46, no. April, p. 112740, 2025, doi: 10.1016/j.mtcomm.2025.112740.

[17] J. Praneeth, S. Venkatesh, and L. S. Krishn, “Process parameters influence on mechanical properties of AlSi10Mg by SLM,” *Materials Today: Proceedings*, no. xxxx, 2023, doi: 10.1016/j.matpr.2022.12.222.

[18] M. Pagac *et al.*, “Prediction of model distortion by fem in 3d printing via the selective laser melting of stainless steel aisi 316l,” *Applied Sciences (Switzerland)*, vol. 11, no. 4, pp. 1–16, 2021, doi: 10.3390/app11041656.

[19] F. Günther *et al.*, “Characterization of additively manufactured lumbar interbody fusion cages based on triply periodic minimal surfaces,” *Materials Today Communications*, vol. 39, no. March, p. 108634, 2024, doi: 10.1016/j.mtcomm.2024.108634.

[20] P. Scheel *et al.*, “Advancing efficiency and reliability in thermal analysis of laser powder-bed fusion,” *International Journal of Mechanical Sciences*, vol. 260, no. June, p. 108583, 2023, doi: 10.1016/j.ijmecsci.2023.108583.

[21] A. Olleak and Z. Xi, “Efficient LPBF process simulation using finite element modeling with adaptive remeshing for distortions and residual stresses prediction,” *Manufacturing Letters*, vol. 24, pp. 140–144, 2020, doi: 10.1016/j.mfglet.2020.05.002.

[22] T. Wu, C. Li, F. Sun, P. F. Liu, and H. B. Xia, “Reduction in residual stress and distortion of thin-walled inconel 718 specimens fabricated by selective laser melting: Experiment and numerical simulation,” *International Journal of Pressure Vessels and Piping*, vol. 212, no. August, 2024, doi: 10.1016/j.ijpvp.2024.105292.

[23] N. Ahmed, I. Barsoum, and R. K. Abu Al-Rub, “Numerical investigation of residual stresses in thin-walled additively manufactured structures from selective laser melting,” *Heliyon*, vol. 9, no. 9, p. e19385, 2023, doi: 10.1016/j.heliyon.2023.e19385.

[24] R. Zhou, H. Liu, and H. Wang, “Modeling and simulation of metal selective laser melting process: a critical review,” *International Journal of Advanced Manufacturing Technology*, vol. 121, no. 9–10, pp. 5693–5706, Aug. 2022, doi: 10.1007/S00170-022-09721-Z/METRICS.

[25] M. R. Condruz, T. A. Badea, and A. Paraschiv, “Numerical and experimental investigation on flexural properties of selective laser melting (SLM) manufactured strut lattices structures from Ti-6Al-4V and Inconel 625,” *Materials Today Communications*, vol. 40, no. August, p. 110150, 2024, doi: 10.1016/j.mtcomm.2024.110150.

[26] A. Yin, W. Yu, W. Zhu, W. Li, V. Ji, and C. Jiang, “Microstructural characterization and wear performance of shot-peened TA15 titanium alloy fabricated by SLM,” *Materials Characterization*, vol. 209, no. September 2023, p. 113747, 2024, doi: 10.1016/j.matchar.2024.113747.

[27] Z. Jiang, P. Xu, Y. Liang, and Y. Liang, “Deformation effect of melt pool boundaries on the mechanical property anisotropy in the SLM AlSi10Mg,” *Materials Today Communications*, vol. 36, no. July, p. 106879, 2023, doi: 10.1016/j.mtcomm.2023.106879.

[28] B. Chen *et al.*, “Comparative study on microstructure, mechanical and high temperature oxidation resistant behaviors of SLM IN718 superalloy before and after heat treatment,” *Journal of Materials Research and Technology*, vol. 31, no. June, pp. 1535–1546, 2024, doi: 10.1016/j.jmrt.2024.06.163.